2024 IEEE International Conference on Robotics and Automation (ICRA 2024)
May 13-17, 2024. Yokohama, Japan

Sensorless Estimation of Contact Using Deep-Learning for Human-Robot Interaction

Shilin Shan[1,*] and Quang-Cuong Pham[2]

***Abstract*— Physical human-robot interaction has been an area of interest for decades. Collaborative tasks, such as joint compliance, demand high-quality joint torque sensing. While external torque sensors are reliable, they come with the drawbacks of being expensive and vulnerable to impacts. To address these issues, studies have been conducted to estimate external torques using only internal signals, such as joint states and current measurements. However, insufficient attention has been given to friction hysteresis approximation, which is crucial for tasks involving extensive dynamic to static state transitions. In this paper, we propose a deep-learning-based method that leverages a novel long-term memory scheme to achieve dynamics identification, accurately approximating the static hysteresis. We also introduce modifications to the well-known Residual Learning architecture, retaining high accuracy while reducing inference time. The robustness of the proposed method is illustrated through a joint compliance and task compliance experiment.**

***Index Terms*— Deep Learning Methods, Physical Human-robot Interaction, Industrial Robots, Dynamics Identification**

I. Introduction

Physical human-robot Interaction has been an area of interest for many years. In collaborative tasks such as joint compliance or task compliance, users are allowed to change the robot configuration by simply pushing the robot link at any position or dragging the robot end-effector. Consequently, external force/torque sensing is crucial for achieving safe and dexterous collaboration. Collaborative robots typically rely on costly and impact-prone joint torque sensors to provide link-level external torque feedback. To address these limitations, external torque approximation based on dynamics identification and internal signals has been studied for years to reduce manufacturing costs and enhance robot control schemes.

Numerous approaches have been proposed, falling into categories such as model-based methods [1]–[5], data-driven model-free methods [6], [7], and hybrid methods [8]–[10]. While these methods have demonstrated promising outcomes in various tasks like trajectory tracking, wrench estimation, and assembly, their primary focus has been on robot dynamics during continuous motions. However, a notable gap exists in the literature concerning the hysteresis error that occurs at zero joint velocity. This scenario is particularly relevant in tasks like joint compliance and task compliance, which involve extensive joint status transitions from static to dynamic and vice versa.

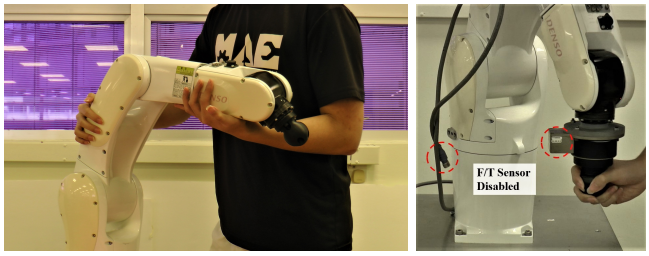

Fig. 1: Snapshot of joint compliance (left) and task compliance (right). A video clip is available in the supplementary or at: https://youtu.be/Yrjf5tU94e8 for higher resolution.

To address this challenge, we propose a Neural-Network-based method with a special input scheme and an enhanced Neural Network structure to achieve dynamics identification at the current level. Specifically, our main contributions can be summarized as follows:

- We designed a special input scheme for the Neural Networks that retains long-term temporal information of essential variables during execution. This is crucial for approximating static hysteresis, which requires non-local memory of joint states.
- We proposed modifications to the well-known Residual Learning method to make it adaptive to robot systems with high system frequency. Such modifications are effective in reducing model inference time while maintaining high accuracy.

We demonstrate the accuracy and reliability of the proposed method through joint compliance based on admittance control and task compliance enabled by wrench estimation.

The paper is organized as follows: In Section II, we discuss the related works on dynamics identification, hysteresis approximation, and Neural Networks. In Section III, we present the concepts for input design and modifications to Residual Learning models. In Section IV, we discuss the data collection procedures and modeling training results with ablation studies. In Section V, we show the model performance in joint compliance and task compliance tasks.

II. Related Works

The study of dynamics identification has been conducted extensively for a variety of applications, including collision

[1] Shilin Shan is with School of Mechanical and Aerospace Engineering, Nanyang Technological University, Singapore (address: 50 Nanyang Ave, Singapore 639798; phone: +65 6790 5568; e-mail: shilin.shan153@gmail.com)

[2] Quang-Cuong Pham is with Eureka Robotics, and School of Mechanical and Aerospace Engineering, Nanyang Technological University, Singapore. (e-mail: cuong@ntu.edu.sg)

[*] Corresponding author: Shilin Shan

detection, joint compliance, and wrench estimation. Model-based approaches, predominantly augmented by Generalized Momentum Observer (GMO) and the Kalman Filter, are designed to approximate torque residuals using either measurable motor-driving torques [1], [2], [11] or electrical current coupled with predetermined motor constants [3], [12]–[14]. However, relying on current introduces additional challenges. Specifically, current signals tend to be noisier than torque measurements, and the motor constants provided by manufacturers are occasionally imprecise for certain robotic models [15], [16].

At low speeds or in static states, robots experience reduced measurement noise but increased frictional issues. For instance, non-zero current readings can occur at zero velocity, even without gravitational influence. Despite its importance, only a handful of studies on dynamics identification have either acknowledged or attempted to model this frictional behavior. In the work by Wahrburg et al. [3], friction errors near zero velocity are modeled as Gaussian noises and are mitigated through the use of Kalman Filter. Meanwhile, Gaz et al. [12], [17] approximate these errors with a sigmoid function, accounting for the continuous transition from negative to positive velocity. Comprehensive studies in [18]–[20] attribute such errors to hysteresis and use the Maxwell Slip (MS) model for identification, which demands long-term, non-local memory of joint states. However, the static hysteresis in one joint appears to be affected by the movements of other joints in our settings (detailed in Section V), posing limitations for isolated hysteresis modeling methods.

Another approach to dynamics identification is model-free methods like Neural-Network-based techniques, which have recently gained extensive attention. Deep learning literature confirms that Neural Networks excel at modeling nonlinear relationships when equipped with suitable architectures and unbiased training data [21]. In the context of robot dynamics, neural networks bypass the need for intricate mathematical analyses by learning optimal solutions from unbiased datasets.

As a result, Neural-Network-based methods are being deployed to simplify or improve the mathematical modeling of robot manipulators. Various NN architectures, such as Multilayer Perceptron (MLP) [6]–[9], [22], Recurrent Neural Networks (RNN) [23], and Convolutional Neural Networks (CNN) [23]–[25], have been adapted for diverse tasks and settings. Notably, Long Short-Term Memory (LSTM) networks have demonstrated effectiveness in capturing and learning temporal patterns, making them a favored choice for approximating hysteresis in various applications [26]–[28].

Algorithm 1 MD Update for Threshold t_i

```
for k = 1 To Number-of-Joint do
    if abs(q̇[k]) ≥ t_i[k] then
        MD[k] = q̇[k]
    end if
end for
```

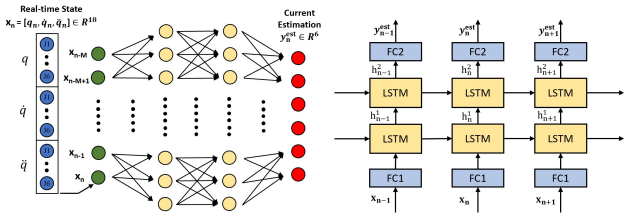

(a) MLP (b) LSTM

Fig. 2: (a) The MLP example featuring two hidden layers, the notations x, y, n, and M represent the input joint states, estimated currents, index of the instantaneous time step, and predefined short-term memory length, respectively. (b) The LSTM example with two LSTM cells, the symbol h denotes the hidden states.

However, for applications involving joint and task compliance, the robot is often required to remain stationary for extended periods without external forces. Using LSTM in these settings poses challenges, especially at high system frequencies (above 200Hz for industrial robots) and when approximating hysteresis based on data from several minutes in the past. In this scenario, two key issues arise: (i) Although LSTM is designed for long-term memory retention, its capacity can wane when recalling information from thousands of frames back. (ii) The recurrent nature of LSTM can lead to output drift, meaning that even with a constant input, the estimation can fluctuate, undermining the model's reliability.

To this end, we are motivated to design an input scheme that keeps a non-vanishing memory of joint states while also ensuring stable estimations. Drawing inspiration from the aforementioned MS model, we introduce in the next section a combination of the proposed input scheme and modified Residual Learning architecture based on MLP.

III. Model Structures and Input Scheme

A. MLP and LSTM

A standard MLP architecture is illustrated in Fig. 2a, consisting of an input layer, multiple fully-connected (FC) hidden layers, and an output layer. While several studies [6], [7] have used instantaneous joint states as input, we enhance the model's memory by including joint states from M consecutive time steps (short-term memory) in the input layer. This idea shares similarities with approaches found in [29], [30]. Based on our observations, this multi-frame input design results in improved estimation accuracy and reduced noise.

The baseline LSTM model can be seen in Fig. 2b. For each recurrent unit, the input is propagated through an encoder, LSTM cells, then an output decoder. Given the trivial patterns of joint states, we use FC layers for encoding and decoding and one recurrent unit for each data frame. Further details in the LSTM cells can be found in [31].

B. Motion Discriminator Input Scheme

The proposed input scheme introduces a global variable called the Motion Discriminator (MD), designed to cap-

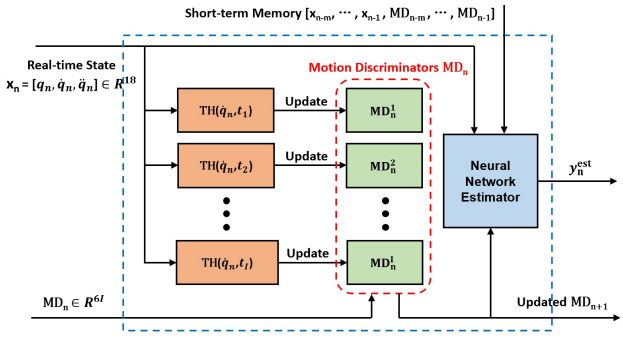

Fig. 3: The block diagram for the Motion Discriminator input scheme. TH(·) and t_i denote the thresholding functions and velocity thresholds.

ture temporal information crucial for enabling Neural Networks to differentiate between static and dynamic behaviors. Specifically, for each frame of joint states, denoted by x_n, we define multiple thresholds $T = (t_1, t_2, \ldots, t_I)$. Each threshold $t_i \in \mathbb{R}^6$ (one element for each joint) is used to update the MD via a thresholding function TH(·), as outlined in Algorithm 1. Alternatively, the update law can be described as follows: if a joint's velocity surpasses a given threshold, the joint is considered non-static and the MD is updated with that velocity value. If the velocity falls below the threshold, no update is made. As a result, when a joint's velocity nears zero, the MD retains the signed value of the threshold. The complete MD is constructed by concatenating I vectors, each generated from a thresholding function.

As previously noted, the MD design draws inspiration from the Maxwell Slip (MS) friction model. As visualized in Fig. 4, the macro friction behavior is modeled by the parallel connection of I elasto-slide elements. The hysteresis friction of an individual element is formulated as follows:

$$\text{If } |z-\zeta_i| < \Delta_i, \text{ then } \begin{cases} F_i = k_i(z-\zeta_i) \\ \zeta_i = \text{constant} \end{cases}$$
$$\text{else } \begin{cases} F_i = \text{sgn}(z-\zeta_i)W_i \\ \zeta_i = z - \text{sgn}(z-\zeta_i)\Delta_i \end{cases} \quad (1)$$

where z is the common displacement input, and $\Delta_i = \frac{W_i}{k_i}$, ζ_i, k_i, and W_i are the saturation displacement, element position, stiffness, and saturation force of the element i. In this formulation, Δ_i serves as a criterion to determine whether an element should follow a sticking or a slipping model. The overall friction is given by the sum of all elementary frictions, which can also be expressed in a specialized manner to better clarify the input-output relationship:

$$F_h = \sum_{i=1}^{I} F_i = \sum_{i=1}^{I} W_i \Phi_i(z_n, \zeta_{ni}, \Delta_{ni}) \quad (2)$$

where $\Phi(\cdot)$ is a nonlinear function described by (1). Given a constant system frequency, utilizing the MD and joint states as NN inputs achieves two key objectives: (i) Building multiple virtual elasto-slide elements, with their sticking/slipping statuses discriminated by the thresholds $\Delta_i = t_i/f$, where f is the system frequency; (ii) Providing the necessary input

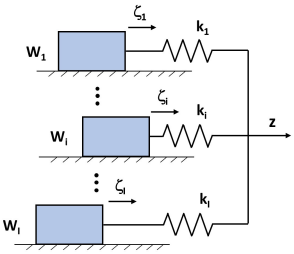

Fig. 4: The Maxwell Slip model of I elasto-slide elements.

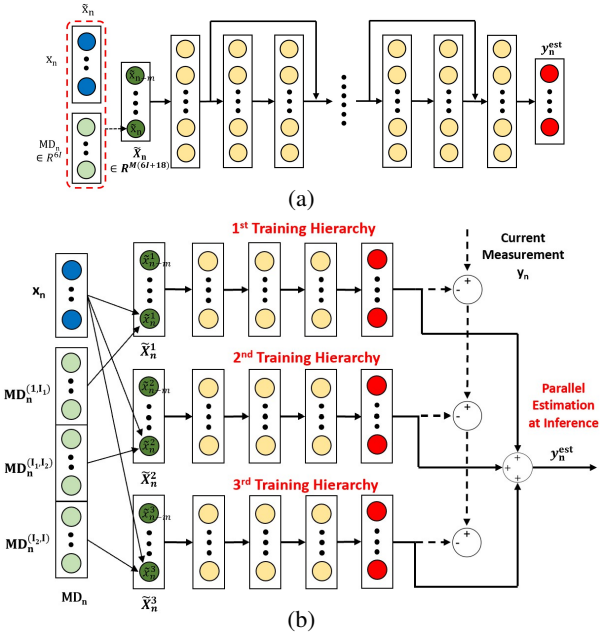

Fig. 5: (a) The classical Residual Learning (RDL) structure. $\tilde{x}$ represents the combined input. (b) The Hierarchical Residual Learning (HRDL) architecture. The dashed and solid lines indicate the data flow in the training phase and during online inference, respectively. The superscripts of MD, e.g., (I_1, I_2), indicate the subset of MD with index from I_1 to I_2.

for MS modeling, i.e., $z_n = q_n$, $\Delta_{ni} = sgn(\dot{q}_n)\Delta_i$, and $\zeta_{ni} = z_n - \Delta_{ni}$.

C. Hierarchical Residual Learning

With an appropriate input scheme, the Neural Network structure should also be selected carefully to reduce inference time while ensuring accuracy. Residual Learning [32], abbreviated as RDL in this paper, is known for mitigating the vanishing gradient problem, thus enabling deep Neural Network structures. When integrated with multi-frame and MD input schemes, an RDL model can be designed for the dynamics identification purpose, as shown in Fig. 5a. However, for general-purpose applications lacking additional computational resources like GPUs, a large number of input frames, velocity thresholds, or hidden layers can result in prolonged inference times, which is problematic for tasks requiring real-time force feedback.

We tackle this issue by transforming the basic Residual Learning architecture into a Hierarchical Residual Learning (HRDL) design, illustrated in Fig. 5. During training, the first

hierarchy processes joint states, a subset of MD, and multi-frame short-term memory through a basic MLP structure to yield an initial current estimation. A new dataset, comprising the error between this estimation and ground truth, is then generated. The second hierarchy, utilizing the same MLP structure but different subsets of MD, is trained on this residual data to refine the initial estimation. Additional hierarchies can be added in a similar fashion, each trained to estimate the residual error of its predecessor. During online inference, all hierarchies operate in parallel, taking advantage of the CPU's multi-core capabilities and ensuring the inference time is bounded by the forward propagation time of a single hierarchy.

This modification is not just applicable to dynamics identification problems; it can also be effective for general tasks requiring both high accuracy and quick inference from deep Neural Networks.

IV. Data Collection and Training

A. Training Data Collection

In model-based methods, rigid body and friction dynamics equations are predefined, allowing for minimal data collection through optimized exciting trajectories [17]. In contrast, data-driven model-free methods, particularly those based on Neural Networks, make no prior assumptions, thus the training results rely solely on the dataset distribution. To address this, we collected data under two scenarios: first, where the robot follows continuous, pre-planned trajectories for predefined tasks; and second, where it responds to random external forces, leading to frequent shifts between static and dynamic joint states.

1) Continuous Trajectory Dataset: The dataset's trajectories were generated using via-point path planning in the task space. Joint velocity and acceleration were obtained from the first and second derivatives of joint position. A third-order Butterworth Filter was applied to minimally reduce signal noise. However, we retained some noise in the dataset, as we believe the NN models should learn from noisy signals to enhance its robustness. Joint states and currents were recorded at a frequency of 100Hz, totaling 1,235,247 frames.

2) Hysteresis-rich Trajectory Dataset: Trajectories in this dataset were generated in the joint space to simulate the on-off behaviors induced by external forces. The generation followed a repetitive algorithm: (i) Random target positions were sampled for each of the six joints; (ii) Joints moved toward these targets at random constant velocities, pausing for 3 seconds after every 3 seconds of execution; (iii) Joints stayed stationary upon reaching their goals until all goals were met. This design aimed to enrich the dataset with interruptions, thereby offering Neural Networks hysteresis information gathered from static scenarios. All data were recorded at 100Hz, totaling 1,865,016 frames.

B. Method Implementation

For the proposed method, we implemented a 3-hierarchy HRDL-MD architecture, with each hierarchy featuring 3 hidden layers of 256 neurons. The short-term memory uses $M = 5$. Through a series of screening experiments, we selected 15 velocity thresholds ($I = 15$) that yielded the highest accuracy. The detailed threshold values and groupings are provided in Table I.

HRDL Thresholds					
Hierarchy	t_1	t_2	t_3	t_4	t_5
1	0.003	0.006	0.009	0.012	0.015
2	0.012	0.016	0.020	0.024	0.028
3	0.002	0.006	0.010	0.014	0.018

TABLE I: Values and groupings of HRDL-MD thresholds.

For baseline comparisons, we used the model-based method proposed in [12]. In particular, we identified dynamics parameters at the current level using sinusoid exciting trajectories and applied the Generalized Momentum Observer (GMO) for current residual approximation in the joint compliance experiment in Section VI.

For the model-free methods, we implemented the basic MLP, LSTM and RDL models. The detailed model depth and layer size are omitted due to limited space, but can be inferred by comparing the inference times listed in Table IIb to the HRDL-MD scheme. All models employed ReLU activation in fully connected layers, except those preceding the output layer. LSTM layers utilized default sigmoid and tanh activations. All models were trained using MSE loss and optimized with the Adam algorithm. Notably, limiting LSTM input to 100-150 frames (1-1.5 seconds of memory) yielded optimal results, while extending input beyond 200 frames reduced accuracy instead.

V. Error Analysis with Ablation Study

The test set included 40% hysteresis-free (continuous) and 60% hysteresis-rich (interrupted) trajectories, totaling 94,490 frames. Qualitative results are visualized in Fig. 6, while Table II(a) provides a quantitative error comparison. Notice that the unit for motor current - percentage use (%Use) of loading capacity - may be less intuitive. Since the manufacturer did not provide motor constants, we used external force-sensing devices to roughly estimate equivalent torques, as detailed in Section VI. For the sake of accuracy comparison, we have adhered to using %Use in this section.

In Fig. 6, triangle and circle markers on the time axis signify when a joint starts and stops rotating, respectively. Lacking temporal information, the RDL model failed to capture hysteresis, leading to significant errors in static states (e.g., after 6s and 26s, for almost all joints). This limitation was also evident in the model-based identification method, despite its effectiveness in dynamic situations. The issue was particularly obvious for Joints 1, 4, and 6, where both methods inaccurately predicted near-zero values due to gravity's absence. Conversely, the LSTM model, equipped with non-local memory, somewhat captured hysteresis but occasionally produced unreliable drifting estimates in static conditions. Finally, integration of the MD input scheme with the RDL model ensured consistent and accurate hysteresis approximation across all scenarios.

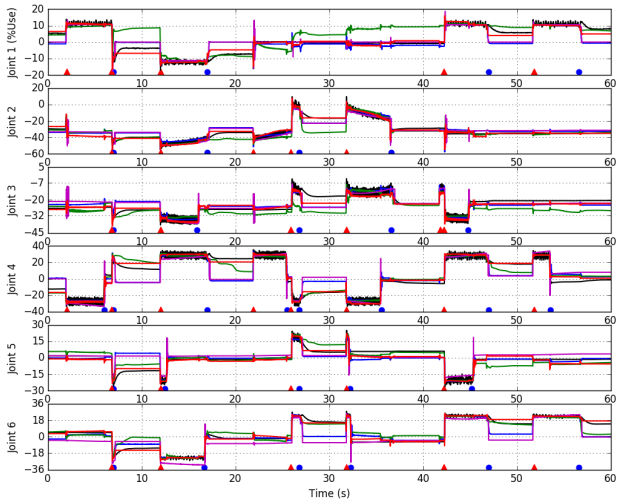

Fig. 6: Comparison of proposed and baseline methods on the hysteresis-rich trajectories. The black line indicates the current measurement. The blue, green, magenta, and red lines correspond to the RDL with short-term memory, LSTM, model-based approach, and RDL-MD scheme, respectively. Triangles and circles on the time axis mark the start and end points of joint rotations.

RMSE (%Use) Comparison across Models							
Method	L-T-Info	J1	J2	J3	J4	J5	J6
Model-based	No	3.92	5.30	3.90	9.60	6.49	8.08
Basic MLP	No	5.33	5.29	4.86	9.58	4.90	7.16
RDL	No	3.87	4.31	3.78	9.37	4.72	7.13
LSTM	Yes	5.72	4.88	4.57	6.78	3.64	5.76
RDL-MD	Yes	**2.49**	**3.90**	3.49	**5.77**	**3.56**	3.55
HRDL-MD	Yes	2.64	4.02	**3.18**	5.84	3.73	**3.53**

(a)

Inference Time (ms)					
	Basic MLP	RDL	LSTM	RDL-MD	HRDL-MD
Time	1.45	1.46	2.21	1.75	**0.77**

(b)

RMSE (%Use) Comparison across Hierarchies						
Hierarchy	J1	J2	J3	J4	J5	J6
1	3.38	4.54	3.77	5.97	4.06	4.20
2	2.70	4.10	3.20	5.87	3.73	3.60
3	**2.64**	**4.02**	**3.18**	**5.84**	**3.73**	**3.53**

(c)

TABLE II: Error analysis on a test data comprising 94,490 frames, which includes both hysteresis-free and hysteresis-rich trajectories. The abbreviation "L-T-Info" stands for Long-term Temporal Information.

As mentioned in Section III, the static hysteresis in one joint can be influenced by the motion states of other joints. This is exemplified in Fig. 6, where Joint 4 is in motion from 31s to 34s. Non-zero hysteresis measurement was present prior to 31s but subsided after 34s. This behavior could be attributed to the ongoing movements of Joints 2 and 3 beyond 34s, which seemingly counteract the hysteresis in Joint 4 through non-trivial mechanisms. Similar cases can also be found for Joint 1 at 22s, Joint 5 at 12s, and Joint 6 at 54s. In such contexts, conventional model-based methods [20], which consider each joint in isolation, is suboptimal as it still yield undesirable non-zero hysteresis approximation.

Deadzone Boundaries						
	J1	J2	J3	J4	J5	J6
Current (%Use)	6.0	6.0	6.0	9.0	11.0	11.0
Torque (Nm)	4.26	4.86	2.42	1.01	1.58	0.84

TABLE III: The deadzone boundaries of current and the equivalent torque calculated with external devices.

From Table II(a), it's evident that the inclusion of long-term temporal information significantly reduces RMSE, particularly for Joints 1, 4, 5, and 6. A comparison between Table II(a) and II(b) reveals that the HRDL-MD scheme achieves the accuracy of the basic RDL-MD model but with quicker inference, thanks to the parallel forward propagation design. Further, Table II(c) indicates that the first hierarchy captures a significant portion of the robot dynamics, with each subsequent hierarchy further reducing error. These findings suggest that a shallow HRDL may be adequate for tasks like collision detection, which require only basic sensing capabilities. On the other hand, tasks that require a higher degree of accuracy, such as wrench estimation for force control, may benefit from a deeper HRDL model.

VI. Applications

A. Joint Compliance with Deadzone Compensation

Joint compliance is vital for facilitating safe and effective human-robot interactions, especially in collaborative settings where a robot needs to dynamically respond to forces applied at unpredictable locations on its body. In the case of position-controlled robots like the Denso-VS060, users are limited in their ability to directly manipulate joint torque or current. A commonly adopted solution, described in [1], involves using an admittance controller, wherein command velocities are set proportional to the residuals as expressed by $\dot{q}_n = K_p(y_n - y_n^{est})$. Although the MD input design substantially mitigates static hysteresis, residual errors from noise and unmodeled dynamics remain. To ensure reliable admittance control, a deadzone is introduced for effective error compensation. Similar methodologies are discussed in [12], which suggests a 10Nm threshold for all joints. However, such a threshold can make the robot feel 'heavy' by activating joints only when large residuals are present. Consequently, it's essential to empirically determine the deadzone thresholds to meet two key criteria: halting the robot immediately upon removal of external forces and making the robot feel possibly 'light'.

The determined deadzone thresholds are presented in Table III. To allow for smoother motion transitions, we have incorporated a linear transition band around each deadzone boundary, effectively mitigating jerky trajectories. We estimated equivalent torque values using end-effector force measurements at specific static postures, taking into account the robot's geometry. These values can also be viewed as the maximum error across all examined joint configurations.

A joint compliance experiment was subsequently carried out using the HRDL-MD estimation. We applied appropriate forces to the robot body, moving each link first separately and then in combination. For safety, constraints were placed

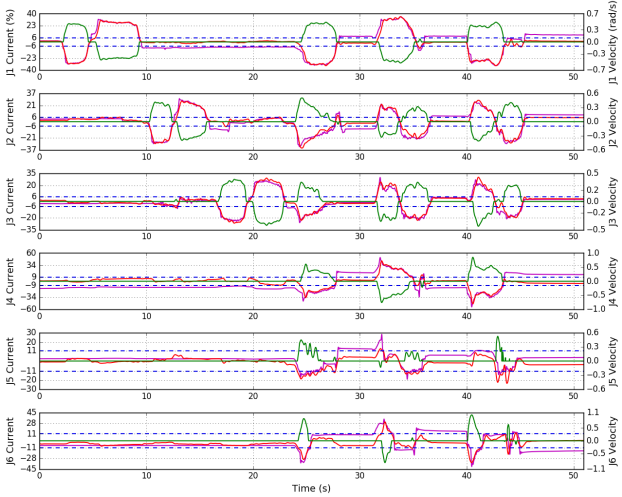

Fig. 7: Filtered residuals in joint compliance task. The red and magenta lines represent the residuals estimated by the proposed HRDL-MD scheme and GMO, respectively. Green lines indicate command velocities, and dashed blue lines mark the deadzone boundaries.

on the command joint positions and velocities. The filtered residuals and corresponding command velocities are illustrated in Fig. 7. GMO estimations are also shown for comparative purposes. It's evident that the GMO scheme without temporal information failed to identify hysteresis, resulting in non-zero residual predictions even in contact-free scenarios. To eliminate these inaccuracies, a wider deadzone would be required, making the robot feel 'heavier'.

B. Task Compliance with Wrench Estimation

Utilizing the current residuals from our HRDL-MD scheme, one could calculate the end-effector wrench via the robot's Jacobian. However, given the noise in current data and the absence of motor constant, we opt for a nonlinear mapping through an additional MLP model. A related study cited in [33] directly used instantaneous current measurements and joint states as Neural Network inputs to estimate external wrench. This method yielded accurate and reliable results in sensorless tight pin insertion tasks. Here, we introduce a compound Neural Network model, as depicted in Fig. 8, which uses the current residuals as its input instead of the raw current measurements.

We conducted a task compliance experiment with a fixed end-effector orientation, using an admittance control scheme in the task space and a carefully chosen deadzone for initiating motion. Figure 9 presents a comparison of two methods along with their respective RMSE values. Notably, the compound-model approach outperforms the single-model method, despite both having the same number of parameters for wrench estimation. The compound-model is particularly effective at capturing peak values more accurately. This improvement can be attributed to the more straightforward residual information extraction by the HRDL-MD scheme.

Interestingly, the hysteresis phenomenon did not significantly impact task compliance. In this case, even the single-

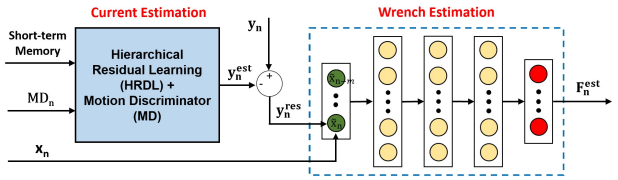

Fig. 8: The compound wrench estimation scheme

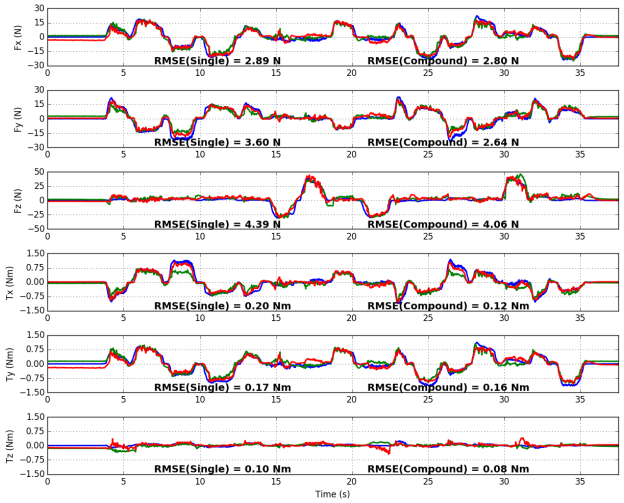

Fig. 9: Comparison among the F/T sensor measurement (blue), single model estimation (green) and compound model estimation (red) in task compliance.

model method, which did not incorporate MD input, can make accurate wrench estimations in static states. This contrasts with other types of robot movements, like decoupled joint rotations, where the baseline method still displayed hysteresis-like errors in estimated wrench. However, the compound Neural Network approach was free of such errors, benefiting from hysteresis compensation at the joint level.

VII. Conclusion

In this paper, we introduced a Neural Network-based approach for dynamic identification using motor current measurement. We designed a Motion Discriminator input scheme, inspired by the Maxwell Slip friction model, to capture long-term joint state information and effectively address the static hysteresis problem. Furthermore, we presented a Hierarchical Residual Learning architecture that enhances estimation accuracy while ensuring short inference times. Our proposed methods have demonstrated promising results in both joint and task compliance scenarios, particularly when complemented by well-formulated control laws and carefully designed deadzones.

One limitation of our study is that the proposed method was implemented under consistent robot dynamics across data collection, training, and validation phases. As a result, the Neural Networks model lacks adaptability to dynamic changes, potentially resulting in inaccurate estimations when a different end-effector is equipped or external devices are attached to the robot. Future work will focus on developing a model fine-tuning or calibration scheme to make the trained model responsive to environmental changes.

REFERENCES

[1] A. De Luca, A. Albu-Schaffer, S. Haddadin, and G. Hirzinger, "Collision detection and safe reaction with the dlr-iii lightweight manipulator arm," in *2006 IEEE/RSJ International Conference on Intelligent Robots and Systems*, pp. 1623–1630, IEEE, 2006.

[2] E. Magrini, F. Flacco, and A. De Luca, "Control of generalized contact motion and force in physical human-robot interaction," in *2015 IEEE international conference on robotics and automation (ICRA)*, pp. 2298–2304, IEEE, 2015.

[3] A. Wahrburg, J. Bös, K. D. Listmann, F. Dai, B. Matthias, and H. Ding, "Motor-current-based estimation of cartesian contact forces and torques for robotic manipulators and its application to force control," *IEEE Transactions on Automation Science and Engineering*, vol. 15, no. 2, pp. 879–886, 2017.

[4] S. Zhang, S. Wang, F. Jing, and M. Tan, "A sensorless hand guiding scheme based on model identification and control for industrial robot," *IEEE Transactions on Industrial Informatics*, vol. 15, no. 9, pp. 5204–5213, 2019.

[5] L. Roveda, A. Bussolan, F. Braghin, and D. Piga, "Robot joint friction compensation learning enhanced by 6d virtual sensor," *International Journal of Robust and Nonlinear Control*, vol. 32, no. 9, pp. 5741–5763, 2022.

[6] N. Yilmaz, J. Y. Wu, P. Kazanzides, and U. Tumerdem, "Neural network based inverse dynamics identification and external force estimation on the da vinci research kit," in *2020 IEEE International Conference on Robotics and Automation (ICRA)*, pp. 1387–1393, IEEE, 2020.

[7] A.-N. Sharkawy, P. N. Koustoumpardis, and N. Aspragathos, "Human–robot collisions detection for safe human–robot interaction using one multi-input–output neural network," *Soft Computing*, vol. 24, no. 9, pp. 6687–6719, 2020.

[8] X. Liu, F. Zhao, S. S. Ge, Y. Wu, and X. Mei, "End-effector force estimation for flexible-joint robots with global friction approximation using neural networks," *IEEE Transactions on Industrial Informatics*, vol. 15, no. 3, pp. 1730–1741, 2018.

[9] J. Hu and R. Xiong, "Contact force estimation for robot manipulator using semiparametric model and disturbance kalman filter," *IEEE Transactions on Industrial Electronics*, vol. 65, no. 4, pp. 3365–3375, 2017.

[10] S. Liu, L. Wang, and X. V. Wang, "Sensorless force estimation for industrial robots using disturbance observer and neural learning of friction approximation," *Robotics and Computer-Integrated Manufacturing*, vol. 71, p. 102168, 2021.

[11] A. De Luca and R. Mattone, "Sensorless robot collision detection and hybrid force/motion control," in *Proceedings of the 2005 IEEE international conference on robotics and automation*, pp. 999–1004, IEEE, 2005.

[12] C. Gaz, E. Magrini, and A. De Luca, "A model-based residual approach for human-robot collaboration during manual polishing operations," *Mechatronics*, vol. 55, pp. 234–247, 2018.

[13] A. Wahrburg, E. Morara, G. Cesari, B. Matthias, and H. Ding, "Cartesian contact force estimation for robotic manipulators using kalman filters and the generalized momentum," in *2015 IEEE International Conference on Automation Science and Engineering (CASE)*, pp. 1230–1235, IEEE, 2015.

[14] L. Roveda, G. Pallucca, N. Pedrocchi, F. Braghin, and L. M. Tosatti, "Iterative learning procedure with reinforcement for high-accuracy force tracking in robotized tasks," *IEEE Transactions on Industrial Informatics*, vol. 14, no. 4, pp. 1753–1763, 2017.

[15] M. Gautier and S. Briot, "Global identification of joint drive gains and dynamic parameters of robots," *Journal of Dynamic Systems, Measurement, and Control*, vol. 136, no. 5, p. 051025, 2014.

[16] T. Xu, J. Fan, Q. Fang, Y. Zhu, and J. Zhao, "Robot dynamic calibration on current level: modeling, identification and applications," *Nonlinear Dynamics*, vol. 109, no. 4, pp. 2595–2613, 2022.

[17] C. Gaz, M. Cognetti, A. Oliva, P. R. Giordano, and A. De Luca, "Dynamic identification of the franka emika panda robot with retrieval of feasible parameters using penalty-based optimization," *IEEE Robotics and Automation Letters*, vol. 4, no. 4, pp. 4147–4154, 2019.

[18] V. Lampaert, J. Swevers, and F. Al-Bender, "Modification of the leuven integrated friction model structure," *IEEE transactions on Automatic Control*, vol. 47, no. 4, pp. 683–687, 2002.

[19] F. Al-Bender, V. Lampaert, and J. Swevers, "The generalized maxwell-slip model: a novel model for friction simulation and compensation," *IEEE Transactions on automatic control*, vol. 50, no. 11, pp. 1883–1887, 2005.

[20] S. Liu, L. Wang, and X. V. Wang, "Sensorless haptic control for human-robot collaborative assembly," *CIRP Journal of Manufacturing Science and Technology*, vol. 32, pp. 132–144, 2021.

[21] M. A. Nielsen, *Neural networks and deep learning*, vol. 25. Determination press San Francisco, CA, USA, 2015.

[22] D. Kim, D. Lim, and J. Park, "Transferable collision detection learning for collaborative manipulator using versatile modularized neural network," *IEEE Transactions on Robotics*, 2021.

[23] M. Hanafusa and J. Ishikawa, "External force estimation for nonlinear systems using recurrent neural network," in *2019 IEEE/ASME International Conference on Advanced Intelligent Mechatronics (AIM)*, pp. 1055–1061, IEEE, 2019.

[24] D.-H. Lee, W. Hwang, and S.-C. Lim, "Interaction force estimation using camera and electrical current without force/torque sensor," *IEEE Sensors Journal*, vol. 18, no. 21, pp. 8863–8872, 2018.

[25] J. Xia and K. Kiguchi, "Sensorless real-time force estimation in microsurgery robots using a time series convolutional neural network," *IEEE Access*, vol. 9, pp. 149447–149455, 2021.

[26] D. Lim, D. Kim, and J. Park, "Momentum observer-based collision detection using lstm for model uncertainty learning," in *2021 IEEE International Conference on Robotics and Automation (ICRA)*, pp. 4516–4522, IEEE, 2021.

[27] D. Wu, Y. Zhang, M. Ourak, K. Niu, J. Dankelman, and E. Vander Poorten, "Hysteresis modeling of robotic catheters based on long short-term memory network for improved environment reconstruction," *IEEE Robotics and Automation Letters*, vol. 6, no. 2, pp. 2106–2113, 2021.

[28] N. Hirose and R. Tajima, "Modeling of rolling friction by recurrent neural network using lstm," in *2017 IEEE international conference on robotics and automation (ICRA)*, pp. 6471–6478, IEEE, 2017.

[29] N. Tran, J. Y. Wu, A. Deguet, and P. Kazanzides, "A deep learning approach to intrinsic force sensing on the da vinci surgical robot," in *2020 Fourth IEEE International Conference on Robotic Computing (IRC)*, pp. 25–32, IEEE, 2020.

[30] T. Zhang, X. Liang, and Y. Zou, "Modeling of robot's low-speed motion nonlinear dynamics based on phase space reconstruction neural network," *Journal of Computational and Nonlinear Dynamics*, vol. 16, no. 9, p. 091003, 2021.

[31] S. Hochreiter and J. Schmidhuber, "Long short-term memory," *Neural computation*, vol. 9, no. 8, pp. 1735–1780, 1997.

[32] K. He, X. Zhang, S. Ren, and J. Sun, "Deep residual learning for image recognition," in *Proceedings of the IEEE conference on computer vision and pattern recognition*, pp. 770–778, 2016.

[33] S. Shan and Q.-C. Pham, "Fine robotic manipulation without force/torque sensor," *IEEE Robotics and Automation Letters*, vol. 9, no. 2, pp. 1206–1213, 2024.